Supplementary Materials

Materials and Methods

Molecular biology

The A_{2A}AR-BRIL-ΔC DNA was synthesized by GenScript with flanking restrictions sites AscI at the 5' end and HindIII at the 3' end. The gene, based on the sequences of the wild type human A_{2A}AR and the thermostabilized apocytochrome b_{562} from *E. coli* (M7W, H102I, K106L), referred to as BRIL (*1*), included the following features: (a) residues Ala1 to Leu106 of BRIL were inserted between Lys209 to Gly218 within the A_{2A}AR ICL3 region. (b) C-terminal residues 317-412 of A_{2A}AR were truncated.

The expression vector, designated as pFastBac1-830400, was a modified pFastBac1 vector (Invitrogen) containing an expression cassette with a BamHI flanked HA signal sequence followed by a FLAG tag at the N-terminus and with a 10xHis tag at the C-terminus. The components of the expression cassette were introduced using standard PCR based site-directed mutagenesis. The expression cassette also contained corresponding restriction sites for AscI and HindIII allowing for the standard restriction digest and subsequent ligation of the synthesized A_{2A}AR-BRIL-ΔC DNA.

For the biochemical characterization, all constructs were digested from the pFastBac1-830400 expression vectors using BamHI and HindIII restriction enzymes. After digestion the inserts were subcloned into pcDNA3.1(-) using the endogenous restriction sites *Bam*HI and *Hind*III and their sequences were verified.

Biochemical characterization

Cell growth and transfection

HEK293 cells were grown in culture medium consisting of Dulbecco's modified Eagle's medium (DMEM) supplemented with 10% newborn calf serum (NCS), 50 µg/ml streptomycin and 50 IU/ml penicillin at 37 °C and 7% CO_2. Cells were subcultured twice a week at a ratio of 1:15 on 10 cm ø plates. Cells were transfected with the indicated plasmids (1 µg each) using the calcium phosphate precipitation method (*2*). All experiments were performed 48 h after transfection.

Cell-surface Receptor Measurement and Enzyme-linked Immunosorbent Assay

Twenty-four hours after transfection, cells were split into 96-well poly-D-lysine-coated plates at a density of 10^5 cells per well. After an additional 24 h, cell-surface receptors were labeled with mouse anti-FLAG (M2) primary antibody (Sigma, 1:1000) in culture medium for 30 min at 37 °C. The cells were then washed once with DMEM supplemented with 25 mM HEPES and then incubated for another 30 min at 37 °C in culture medium supplemented with horseradish peroxidase-conjugated anti-mouse IgG produced in goat (Brunswig) (1:5000) as the secondary antibody. The cells were washed twice with phosphate-buffered saline (PBS). Finally, the cells were incubated with 3,3',5,5'-tetramethylbenzidine (TMB) for 5 min in the dark at room temperature. The reaction was stopped with 1M H_3PO_4 and after 5 min the absorbance was read at 450 nm using a VICTOR2 plate reader (PerkinElmer Life Sciences). Control experiments were performed in which no secondary or primary antibody was added. In both cases no absorbance was observed.

Competition Binding Assays using HEK293 cell membranes

[^{3}H]ZM241385 (27.4 Ci/mmol) and [^{3}H]NECA (18.6 Ci/mmol) were obtained from ARC Inc. (St. Louis, MO, USA) and PerkinElmer (Groningen, The Netherlands), respectively. ZM241385 and CGS21680 were obtained from Ascent Scientific (Bristol, UK), while UK432,097 was obtained from Axon (Groningen, The Netherlands). Amiloride was obtained from Sigma Aldrich (Zwijndrecht, The Netherlands). All other materials were purchased from commercial sources and were of the highest available purity.

HEK293 cells were grown and transfected as described above. Membranes were prepared as follows. Cells were detached from plates 48 h after transfection by scraping them into 5 ml PBS, collected and centrifuged at 700 ×g (3000 r.p.m.) for 5 min. Pellets derived from 8 plates (10 cm ø) were pooled and resuspended in 8 ml of ice-cold assay buffer (50 mM Tris-HCl supplemented with 5 mM $MgCl_2$, pH 7.4). An UltraThurrax was used to homogenize the cell suspension. Membranes and the cytosolic fraction were separated by centrifugation at 100,000 ×g (31,000 r.p.m.) in a Beckman Optima LE-80K ultracentrifuge at 4 °C for 20 min. The pellet was resuspended in 4 ml of Tris buffer and the homogenization and centrifugation step was repeated. Assay buffer (2 ml) was used to resuspend the pellet and adenosine deaminase (ADA) was added (0.8 IU/ml) to break down endogenous adenosine. Membranes were stored in 250 µL aliquots at -80 °C. Membrane protein concentrations were measured using the BCA (bicinchoninic acid) method (*3*). For competition binding experiments with [^{3}H]ZM241385, 25 µg of membranes were used at first for the single point experiments, while subsequently between 6 and 20 µg of protein was used for the experiments with whole curves to ensure that total binding was less than 10% of the total radioactivity added to prevent radioligand depletion. For

[^{3}H]NECA competition binding experiments, 30 µg and 50 µg of membranes with transiently expressed A_{2A}AR-WT and A_{2A}AR-BRIL-ΔC were used, respectively. Membrane aliquots were incubated in a total volume of 100 µl of assay buffer at 25 °C for 2 h. Radioligand displacement experiments were performed using five concentrations of competing ligand (ZM241385 or UK432,097) in the absence and presence 1M NaCl or single concentrations of amiloride (100 µM), NaCl (150 mM), combinations thereof or choline chloride (150 mM). [^{3}H]ZM241385 and [^{3}H]NECA were used at a concentration of ~ 4.0 nM and ~ 7.5 nM, respectively. Nonspecific binding was determined in the presence of 100 µM CGS21680 ([^{3}H]ZM241385) or 10 µM ZM241385 ([^{3}H]NECA) and represented less than 15% of the total binding. Incubations were terminated by rapid vacuum filtration to separate the bound and free radioligand through 96-well GF/B filter plates using a Filtermate-harvester (PerkinElmer Life Sciences). Filters were subsequently washed three times with ice-cold assay buffer. The filter-bound radioactivity was determined by scintillation spectrometry using the PE 1450 Microbeta Wallac Trilux scintillation counter (PerkinElmer Life Sciences).

Demonstration of downstream signaling by intracellular cAMP determination.

HEK293T cells were grown and transfected as described above. Cells were harvested 48 h after transfection and the amount of cAMP produced was determined with the LANCE Ultra cAMP 384 kit following the recommended protocol (PerkinElmer Life Sciences). In short, 4000 cells/well were pre-incubated with single concentrations of either UK432,097 (30 nM, approx. EC_{80}) in the absence or presence of ZM241385 (100 nM, approx. 100 × K_i) or ZM241385 (100 nM) alone for 30 min at 37 °C in stimulation buffer (PBS supplemented with 5 mM HEPES, 0.1% BSA, 50 µM rolipram, 50 µM cilostamide and 0.8 IU/ml ADA).

Subsequently, detection and antibody solutions were added according to manufacturer's instructions, which were followed by an incubation of 1 h at room temperature in the dark. The generated fluorescence intensity was quantified on the EnVision® Multilabel Reader (PerkinElmer, Groningen, Netherlands).

Receptor expression in *Sf*9 cells and purification

High-titer recombinant baculovirus (>10^8 viral particles per ml) was obtained using the Bac-to-Bac Baculovirus Expression System (Invitrogen). Briefly, recombinant baculoviruses were generated by transfecting 5 µg of recombinant bacmid containing the target gene sequence into *Spodoptera frugiperda* (*Sf*9) cells using 3 µl of FuGENE HD Transfection Reagent (Roche) and Transfection Medium (Expression Systems). Cell suspension was incubated for 4 d while shaking at 27 °C. P0 viral stock was isolated after 4 d and used to produce high-titer baculovirus stock. Viral titers were performed by flow-cytometric method after staining cells with gp64-PE (Expression Systems) (*4*). *Sf*9 cells at a cell density of 2-3 × 10^6 cells/ml were infected with P2 virus at MOI (multiplicity of infection) of 3. Cells were harvested by centrifugation at 48 h post infection and stored at -80 °C until use.

Insect cell membranes were disrupted by thawing frozen cell pellets in a hypotonic buffer containing 10 mM HEPES (pH 7.5), 10 mM $MgCl_2$, 20 mM KCl and an EDTA-free complete protease inhibitor cocktail (Roche). Extensive washing of the isolated raw membranes was performed by repeated dounce homogenization and centrifugation in the same hypotonic buffer (~2-3 times), and then in a high osmotic buffer containing 1.0 M NaCl, 10 mM HEPES (pH 7.5), 10 mM $MgCl_2$, 20 mM KCl (~3-4 times) to remove soluble and membrane associated

proteins. Purified membranes were resuspended in 10 mM HEPES (pH 7.5), 10 mM $MgCl_2$, 20 mM KCl, and 40% glycerol, flash-frozen in liquid nitrogen and stored at -80 °C until further use.

Prior to solubilization, purified membranes were thawed on ice in the presence of 4 mM theophylline (Sigma), 2.0 mg/ml iodoacetamide (Sigma), and an EDTA-free complete protease inhibitor cocktail (Roche). After incubation for 30 min at 4 °C, membranes were solubilized by incubation in the presence of 0.5% (w/v) *n*-dodecyl-*β*-D-maltopyranoside (DDM) (Anatrace) and 0.1% (w/v) cholesteryl hemisuccinate (CHS) (Sigma) for 2.5-4 h at 4 °C. The unsolubilized material was removed by centrifugation at 150,000 ×g for 45 min. The supernatant was incubated with TALON IMAC resin (Clontech) in the buffer containing 50 mM HEPES (pH 7.5), 800 mM NaCl, 0.5% (w/v) DDM, 0.1% (w/v) CHS, and 20 mM imidazole. After overnight binding, the resin was washed with ten column volumes of 50 mM HEPES (pH 7.5), 800 mM NaCl, 10% (v/v) glycerol, 25 mM imidazole, 0.1% (w/v) DDM, 0.02% (w/v) CHS, 10 mM $MgCl_2$, 8 mM ATP (Sigma) and 25 μM ZM241385 (Tocris, prepared as 100 mM stock in DMSO), followed by four column volumes of 50 mM HEPES (pH 7.5), 800 mM NaCl, 10% (v/v) glycerol, 50 mM imidazole, 0.05% (w/v) DDM, 0.01% (w/v) CHS and 25 μM ZM241385. The receptor was eluted with 25 mM HEPES (pH 7.5), 800 mM NaCl, 10% (v/v) glycerol, 220 mM imidazole, 0.025% (w/v) DDM, 0.005% (w/v) CHS and 25 μM ZM241385 in a minimal volume. Purified receptor in the presence of ZM241385 was concentrated from ~0.4 mg/ml to 60 mg/ml with a 100 kDa molecular weight cut-off Vivaspin concentrator (GE Healthcare). Receptor purity and monodispersity was followed using SDS-PAGE and analytical size exclusion chromatography (aSEC).

Thermostability assays

A_{2A}AR-BRIL-ΔC receptor construct was purified in the apo form as described above except for using KCl instead of NaCl. N-[4-(7-diethylamino-4-methyl-3-coumarinyl)phenyl]maleimide (CPM) dye (Invitrogen) was dissolved in DMSO (Sigma) at 4 mg/mL and stored at −80°C. Before use the CPM stock solution was thawed and diluted 1:40 in dye dilution buffer (10 mM HEPES pH 7.50, 10% glycerol, 0.05% DDM). The thermal denaturation assay (*5*) was performed with total volume of 200 µL sample in a quartz fluorometer cuvette (Starna Cells, Inc., Atascadero, CA). Receptor (4 µg) was diluted in assay buffer (10 mM Hepes pH 7.5, 0.05% DDM, 0.01% CHS) with and without different concentrations and combinations of NaCl, amiloride and ZM241385 to a final volume of 200 µL. Effects of CHS were measured using a modified assay buffer (10 mM Hepes pH 7.5, 800 mM NaCl, 0.05% DDM). 5 µL of the diluted dye was added to the protein containing assay solution and incubated for 30 min at 4°C. The mixed solution was transferred to the cuvette and the data were collected by a Cary Eclipse spectrofluorometer (Varian, USA) with a temperature ramping rate at 2°C/min. The excitation wavelength was 387 nm and the emission wavelength was 463 nm. All assays were performed over a temperature range starting from 20°C and 90°C. The stability data were processed with GraphPad Prism program (GraphPadPrism, Graphpad Sofware, San Diego, CA, USA).

Crystallization

Protein samples of A_{2A}AR-BRIL-ΔC in complex with ZM241385 were reconstituted into lipidic cubic phase (LCP) by mixing with molten lipid using a mechanical syringe mixer (*6*). The protein-LCP mixture contained 40% (w/w) protein solution, 54% (w/w) monoolein (Sigma) and 6% (w/w) cholesterol (AvantiPolar Lipids). Crystallization trials were performed in 96-well

glass sandwich plates (*7*) (Marienfeld) by an NT8-LCP crystallization robot (Formulatrix) using 40-50 nl protein-laden LCP overlaid with 0.8 μl precipitant solution in each well, and sealed with a glass coverslip. Protein reconstitution in LCP and crystallization trials were carried out at room temperature (~21-23 °C). The crystallization plates were stored and imaged in an incubator/imager (RockImager 1000, Formulatrix) at 20 °C. Diffraction quality crystals of an average size of 60×10×3 μm were obtained within 7 days in 25-28% (v/v) PEG 400, 0.04 to 0.06 M sodium thiocyanate, 2% (v/v) 2,5-hexanediol, 100 mM sodium citrate pH 5.0. Crystals were harvested directly from LCP using 50 μm MiTeGen micromounts and immediately flash frozen in liquid nitrogen without adding an extra cryoprotectant.

X-ray data collection and processing

Crystallographic data were collected on the 23ID-B/D beamline (GM/CA CAT) of the Advanced Photon Source at the Argonne National Laboratory using a 10 μm collimated minibeam at a wavelength of 1.0330 Å and a MarMosaic 300 detector. To reduce radiation damage crystals were translated to a fresh position, if possible, or replaced after collecting 5 frames at 3 s exposure and 0.5° oscillation with an unattenuated beam. Datasets from 55 crystals were integrated, scaled and merged together using HKL2000 (*8*).

Structure determination and refinement

Initial molecular replacement solution was obtained by Phaser (*9*) using the A_{2A}AR domain of the A_{2A}AR-T4L-ΔC/ZM structure (PDB ID 3EML) as a search model. BRIL residues were built manually in the excessive ΣA-weighted $2|F_o|-|F_c|$ density by repetitive cycling between Coot (*10*) and Refmac5 (*11*) and the resulting model was further refined using the same

procedure until convergence. Excellent electron densities observed for all cholesterols allowed for reliable distinction of this type of molecule from other protein-bound lipids and for their confident placements and orientations (fig. S10). Electron densities for other lipids, however, were not sufficiently clear to unambiguously identify their headgroups. Therefore, most of the elongated electron density tubes near the protein hydrophobic surface were modeled as oleic acids (OLA), with the exception of few that were better fit with monooleins (OLC), the major lipid component used for crystallization.

The number of water molecules in the interior of the receptor was counted using the following criteria. In vertical direction the boundary was defined by the planes parallel to the membrane (as predicted for A_{2A}AR by OPM server) and passing through Cα atoms of residues Ile3 (extracellular end of helix I) and Ile106 (intracellular end of helix IV). In the plane of the membrane, only water molecules lying within the 7TM helical bundle were counted.

The data collection and refinement statistics are shown in Table S1. Figures were created using *PyMOL* (Schroedinger) and *ICM* (Molsoft).

Modeling of amiloride and derivatives.

Docking of amiloride and its derivatives was performed using an all-atom flexible receptor docking algorithm in ICM-Pro (MolSoft LLC, San Diego) molecular modeling package as described previously (*12, 13*). Chemical structures of amiloride derivatives 5-(N,N-dimethyl)amiloride (DMA), 5-(N,N-hexamethylene)amiloride (MIBA), 5-(N,N-hexamethylene)-amiloride (HMA) were previously described in refs (*14, 15*). Internal coordinate (torsion) movements were allowed in the side chains of the binding pocket, defined as residues within 10Å distance of Na^+ ion in the crystal structure. Other side chains and the backbone of the

protein were kept as in the crystal structure. An initial conformation for each of the ligands was generated by Cartesian optimization of the ligand model in MMFF force field (*16*). Definition of the ligand torsion angles included flexibility in N,N- hexamethylene ring of HMA. Docking was performed by placing the ligand in a random position within 5 Å from the binding pocket and global conformational energy optimization of the complex in internal coordinates (*12, 13*). In the initial 10^6 steps of optimization, ligand movement was limited to a sphere, defined by a 5 Å 'distance restraint' between the guanidine group of the ligand and carboxyl of Asp52$^{2.50}$ side chain; the restraint was removed in the final 10^6 steps. To facilitate side chain rotamer switches in the flexible model of the A_{2A}AR, the first 10^6 steps of the ICM Monte Carlo (MC) procedure used ''soft'' van der Waals (vdW) potentials and high MC temperature, the final 10^6 steps used ''exact'' vdW potentials and gradually decreasing temperature. At least 10 independent runs of the docking procedure were performed for each A_{2A}AR-ligand complex. The docking results were considered ''consistent'' when at least 80% of the individual runs resulted in conformations clustered within a RMSD of <1 Å to the overall best energy pose of the ligand. All calculations were performed on a 12-core Linux workstation.

Supplementary Tables:

Table S1. X-ray data collection and refinement statistics.

Structure	A_{2A}AR-BRIL-ΔC
Data collection	
Number of crystals	55
Space group	*C222₁*
Cell dimensions	
a, b, c (Å)	39.44, 179.52, 140.31
Number of reflections measured	176,392
Number of unique reflections	44,413
Resolution (Å)	29.73 – 1.80 (1.86 - 1.80)
R_{merge}	0.10 (0.81)
Mean I/σ(I)	17.7 (1.8)
Completeness (%)	95.1 (92.8)
Redundancy	4.0 (3.3)
Refinement	
Resolution (Å)	29.73 – 1.80
Number of reflections (test set)	42,032 (2,222)
R_{work} / R_{free}	0.17 / 0.21
Number of atoms	
Proteins	3,110
Ligand (ZM241385)	25
Lipids	441
Na^+	1
Other	199
Average *B* value (Å^2)	
A_{2A}AR	25.3
BRIL	56.0
Ligand (ZM241385)	20.4
Lipids	45.4
Na^+	28.0
Other	37.4
R.m.s. deviations	
Bond lengths (Å)	0.014
Bond angles (°)	1.57
Ramachandran plot statistics (%)*	
Most favored regions	99.5
Additionally allowed regions	0.5
Disallowed regions	0.0

* As defined in MolProbity (*17*).

Table S2. Displacement of specific [^{3}H]ZM241385 binding from A_{2A}AR constructs transiently expressed on HEK293 cell membranes.

Construct	UK432,097	UK + 1M NaCl	ZM241385	ZM + 1M NaCl
	K_i ± SEM (nM)	K_i ± SEM (nM)	K_i ± SEM (nM)	K_i ± SEM (nM)
A_{2A}AR-WT	5.4 ± 1.3	53 ± 9.4**	1.7 ± 0.28	1.4 ± 0.40
A_{2A}AR -ΔC	5.3 ± 1.5	70 ± 15*	1.5 ± 0.31	1.1 ± 0.058
A_{2A}AR -BRIL-ΔC	3.6 ± 0.22	25 ± 1.2***	1.7 ± 0.21	1.2 ± 0.12

Differences in K_i values were analyzed by a Student's t-test. Significant differences were observed for the effect of NaCl on UK432,097 and are noted as follows: * $p < 0.05$, ** $p < 0.01$, *** $p < 0.001$. UK432,097 and ZM241385 binding to A_{2A}AR-ΔC and A_{2A}AR-BRIL-ΔC was not significantly different from A_{2A}AR-WT. Moreover, there was no significant effect of NaCl on ZM241385 binding.

Values are means (± SEM) of three separate experiments performed in duplicate.

Supplementary Figures:

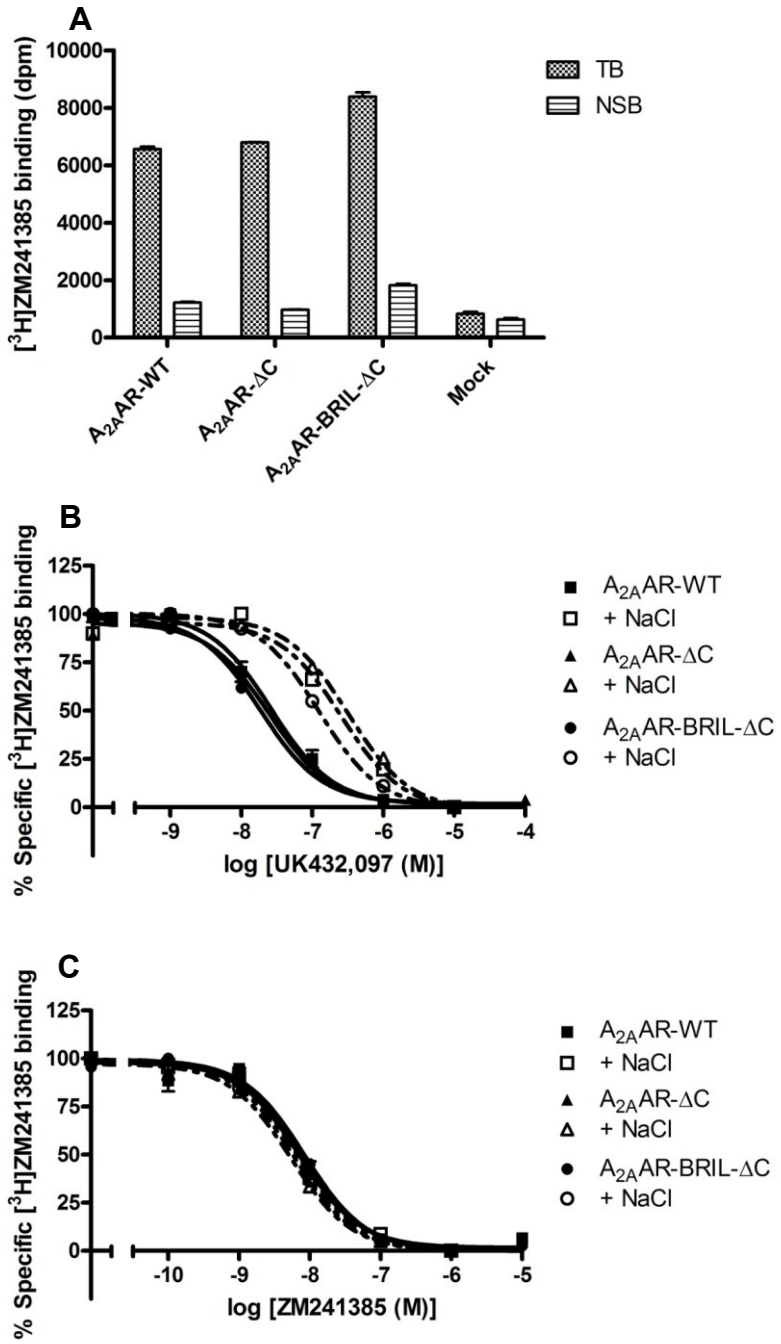

Figure S1. Biochemical characterization of A_{2A}AR constructs. (A) [^{3}H]ZM241385 equilibrium binding to different A_{2A}AR constructs transiently expressed on HEK293 cell membranes in the presence of buffer (total binding, TB) or 100 μM CGS21680 (non-specific binding, NSB). (**B)** Displacement of [^{3}H]ZM241385 in different A_{2A}AR constructs transiently expressed on HEK293 cell membranes by UK432,097 in the absence (filled symbols and solid lines) and presence (open symbols and dashed lines) of 1M NaCl. The figure shown represents

data combined from three separate experiments performed in duplicate. (**C)** Displacement of [^{3}H]ZM241385 in different A_{2A}AR constructs transiently expressed on HEK293 cell membranes by ZM241385 in the absence (filled symbols and solid lines) and presence (open symbols and dashed lines) of 1M NaCl. The figure shown represents data combined from three separate experiments performed in duplicate.

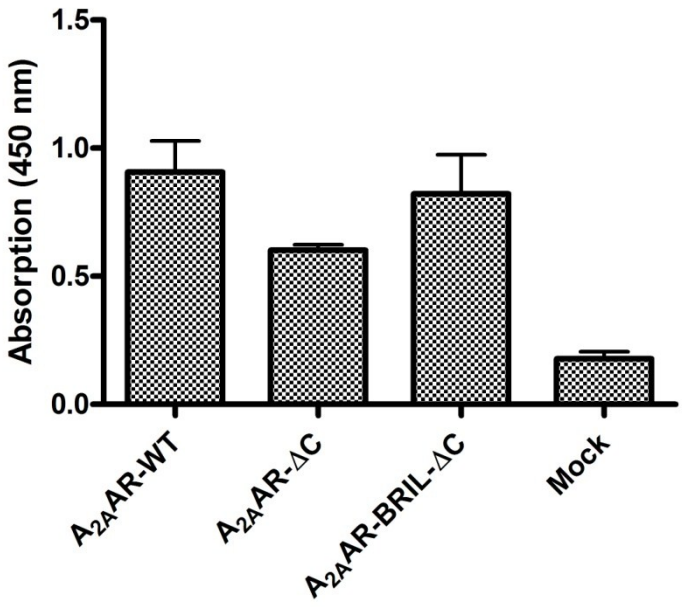

Figure S2. A_{2A}AR constructs expression at the cell surface of HEK293 cells. Whole cell ELISA experiment using a monoclonal anti-FLAG (M2) antibody demonstrates cell surface expression of all constructs in transiently transfected HEK293 cells (mock transfection for reference purposes). The BRIL insertion construct expressed equally well as the wild-type receptor, apparently not causing any problem with the endoplasmic reticulum (ER) quality assurance system.

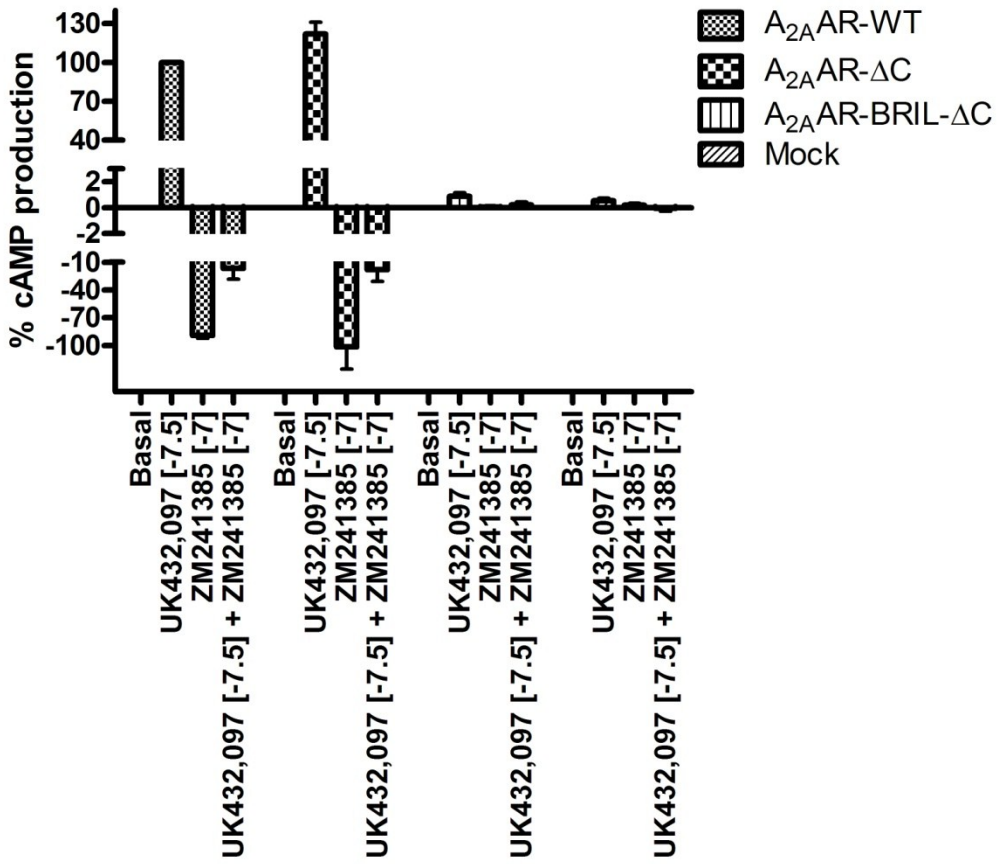

Figure S3. Downstream signaling in A_{2A}AR constructs. cAMP production was determined in HEK293 cells transiently transfected with indicated A_{2A}AR constructs or mock transfection. Basal level was set at 0% for all conditions, while 100% was defined by UK432,097 stimulated cAMP production at A_{2A}AR-WT. ZM241385 behaved as an inverse agonist, as it inhibited the production of cAMP, whether induced by the agonist or as the result of the constitutive activity. The figure shown represents data from three separate experiments performed in duplicate.

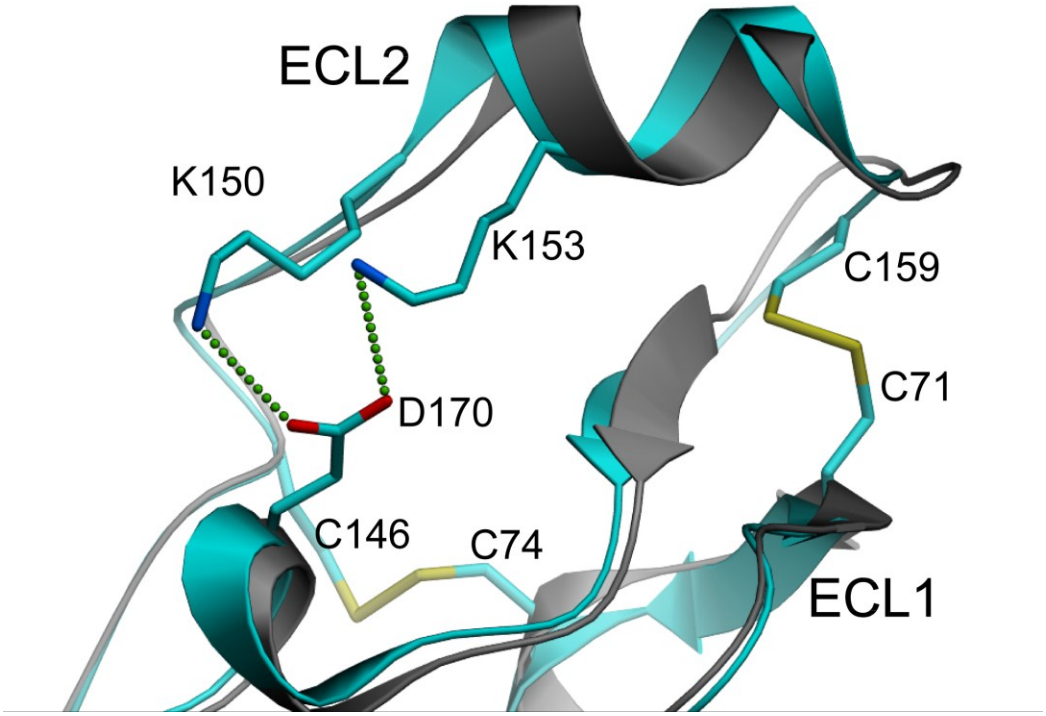

Figure S4. Comparison of ECL2 conformations. Superposition of ECL2 region between the inactive state structure of A_{2A}AR-BRIL-ΔC/ZM241385 (cyan) and the active-like state structure of a thermostabilized A_{2A}AR/NECA (PDB ID 2YDV, grey). Salt bridges are shown as green dotted lines. The fact that a similar conformation of this ECL2 helix was obtained for different constructs and crystal packing in both inactive and active-like states suggests that this is a stable motif, which, however, possesses a certain degree of freedom as it is attached to flexible linkers. Although the functional relevance of this distal α-helix is not yet clear, its secondary structure restricts the orientations of $Lys150^{ECL2}$ and $Lys153^{ECL2}$, which point towards the entrance of the binding pocket and can play a role in initial ligand association and movement to the binding site in addition to defining subtype selectivity of some ligands (*18*).

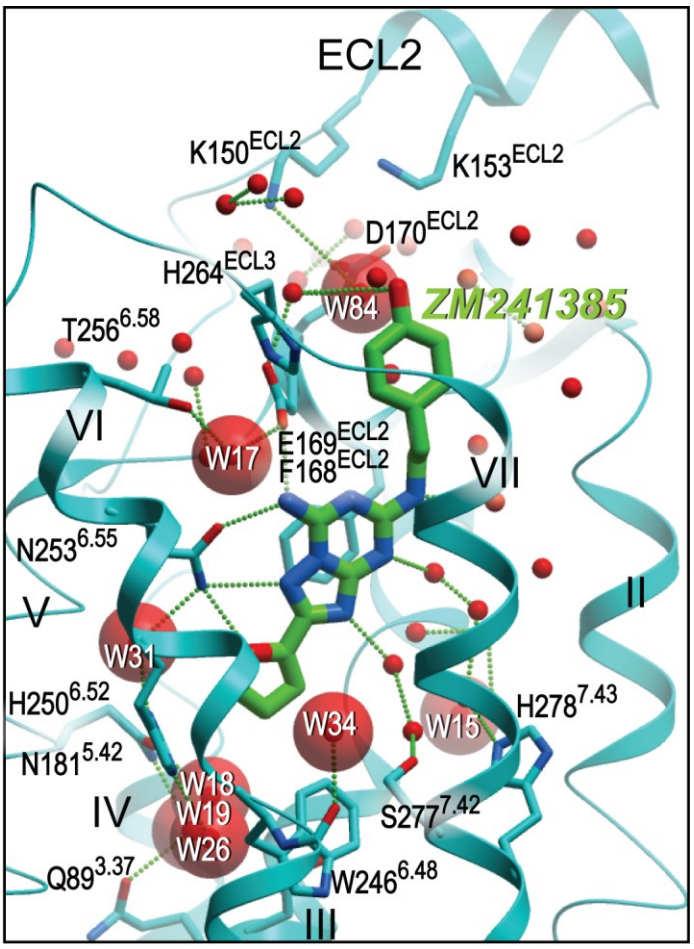

Figure S5. Effect of structured water and ECL2 conformation on A_{2A}AR ligand binding. A_{2A}AR structure is shown in cyan ribbon and sticks for the side chains important for polar interactions with the ligand (ZM241385, green carbons) and with structured water (small red spheres). Important water molecules, mentioned in text are shown as large semi-transparent red spheres and labeled. Hydrogen bonds are shown by green dotted lines. In addition to the previously described water molecule coordinated by Asn253$^{6.55}$ and His250$^{6.52}$ (W31), a cluster of three waters (W18, W19 and W26) is found underneath the ZM241385 ligand, coordinated by His250$^{6.52}$, Asn181$^{5.42}$ and Gln89$^{3.37}$, all of which are important for binding pocket selectivity and potentially involved in receptor activation.

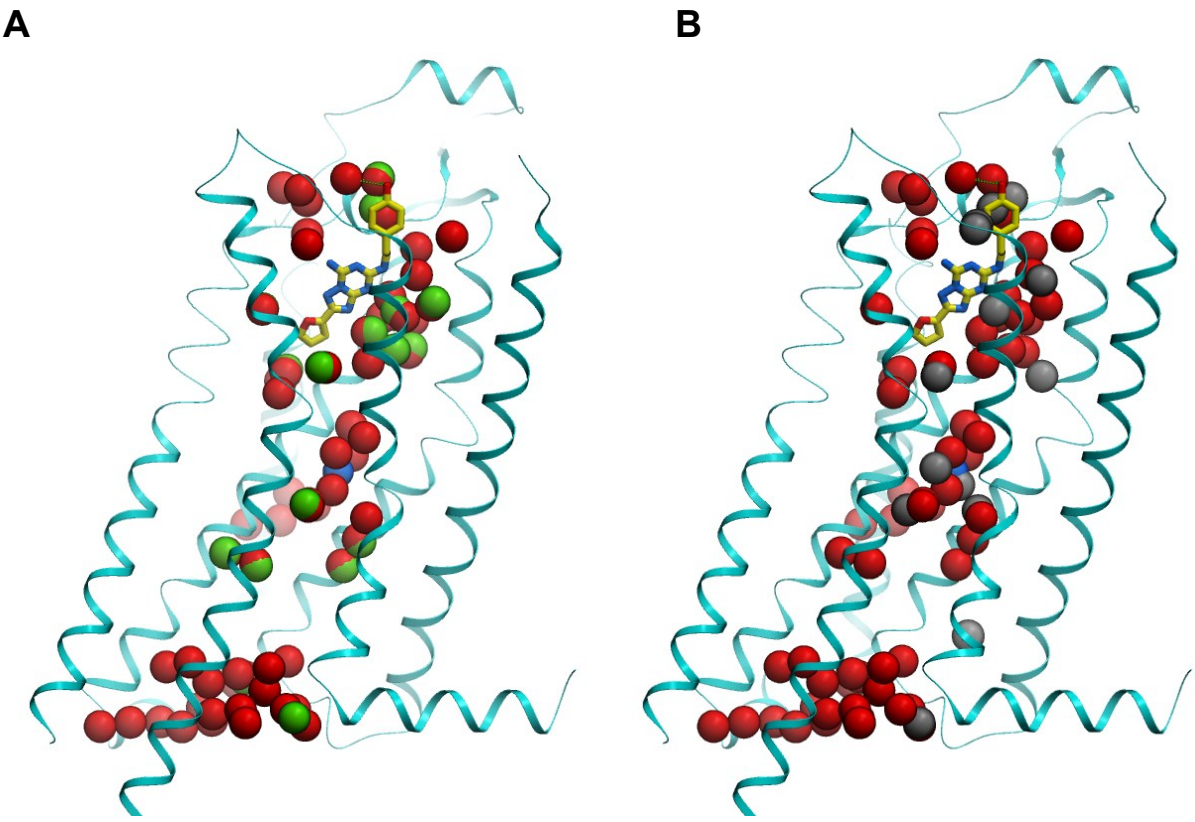

Figure S6. Conserved interior water molecules in GPCR structures. Internal ordered water molecules (red spheres) in A_{2A}AR-BRIL-ΔC/ZM241385 structure (cyan ribbon) are compared with (**A**) ordered waters in A_{2A}AR-T4L-ΔC/ZM241385 (PDB ID 3EML, resolution 2.6 Å, 19 interior water molecules, green spheres), showing a close overlap of 7 water molecules in the EC cluster, and of 3 molecules in the central cluster; and with (**B**) ordered waters in the dark state bovine rhodopsin structure (PDB ID 1U19, resolution 2.2 Å, 14 interior water molecules, grey spheres). While there is no substantial overlap in the EC cluster, rhodopsin structure has 4 conserved waters in the central cluster. Sodium ion in the central cluster is shown as a blue sphere. For clarity, water molecules on the exterior surface of the receptors are not shown.

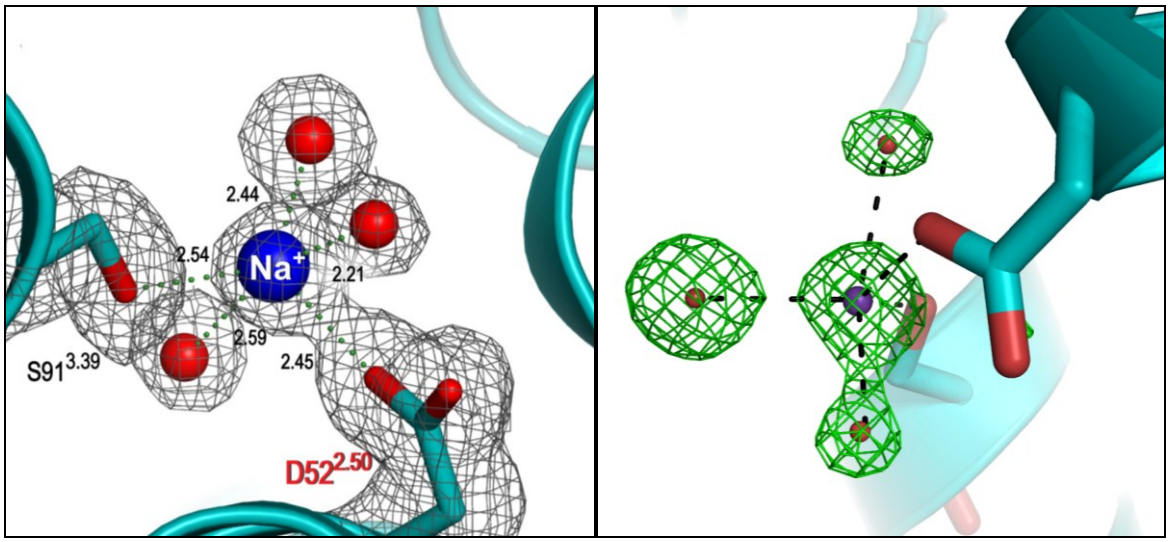

Figure S7. Electron density maps around the Na^+ binding site. (**A**) 2|Fo|-|Fc| electron density for the Na^+ ion, coordinated by $A_{2A}AR$ side chains and water molecules (contoured at 1 σ level). Distances in Å are shown with dashed black lines. (**B**) Simulated annealing (5000 K) omit ($|F_o|$-$|F_c|$) map for sodium ion and coordinating waters contoured at 2σ level, calculated by Phenix (*19*).

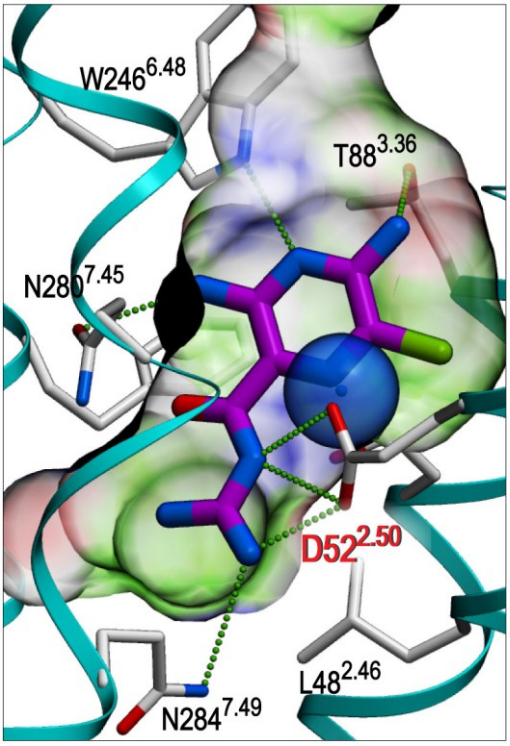

Figure S8. Docking of amiloride in the Na+ binding pocket of A_{2A}AR. Amiloride is shown as sticks with magenta carbons, A_{2A}AR backbone as cyan ribbon and flexible side chains as sticks with white carbons. Position of the Na^+ in the crystal structure is shown as a semitransparent blue sphere.

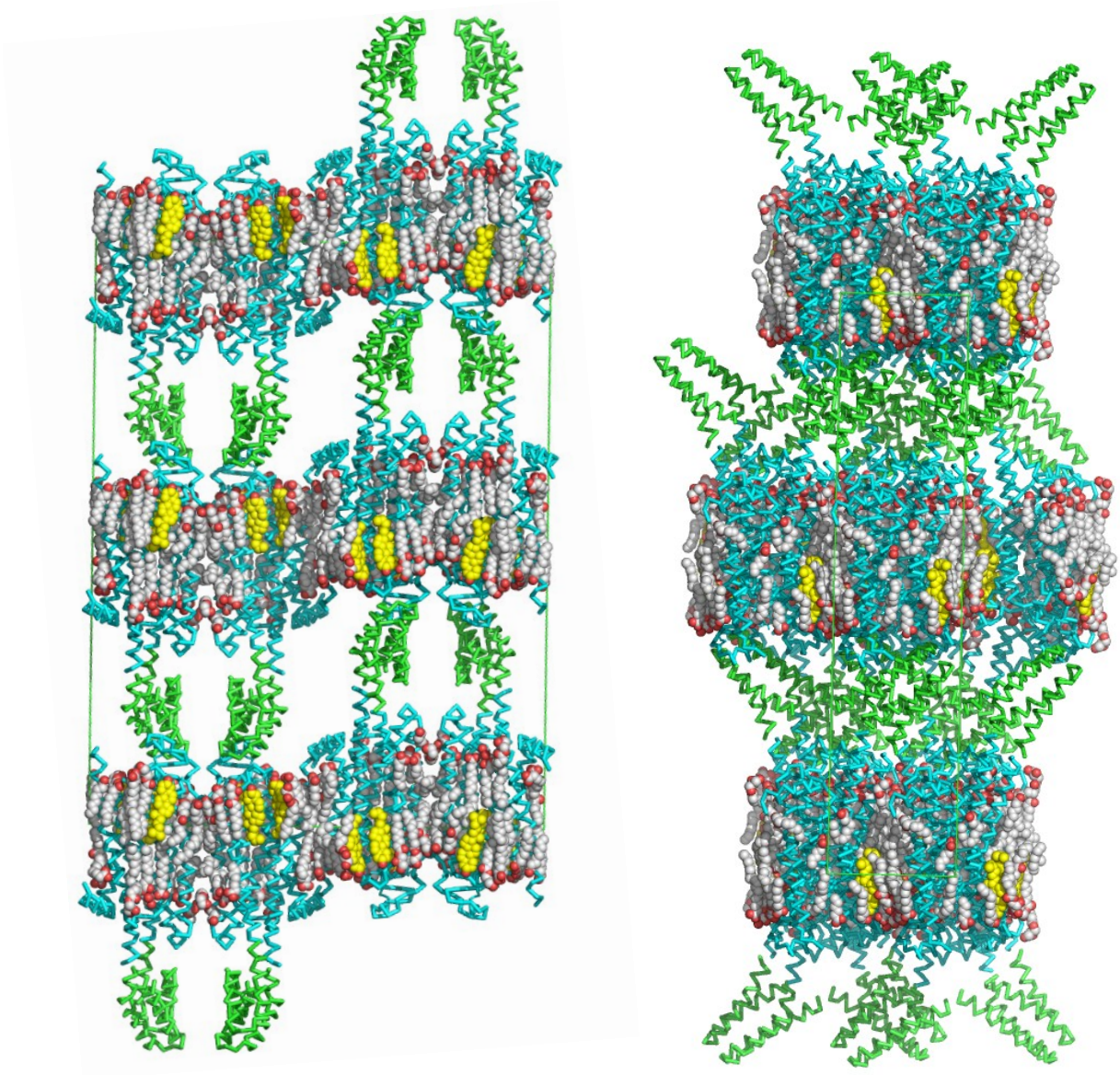

Figure S9. Crystal packing of A_{2A}AR-BRIL-ΔC/ZM241385 crystallized in LCP. The receptor was crystallized in orthorhombic $C222_1$ space group forming layered type I crystal packing (consistent with other LCP grown crystals (*20*)), containing one protein, one ligand, one sodium ion, three cholesterols, 23 lipid chains and 177 water molecules in the crystallographic asymmetric unit. A relatively low solvent content of this crystal form (51%, including lipids) correlates well with the high resolution diffraction. For comparison, the solvent content of several other GPCR crystal forms is 57% (A_{2A}AR-T4L-ΔC/ZM241385, 2.6 Å), 59% (A_{2A}AR-T4L/UK432097, 2.7 Å) and 63% (dopamine D3R-T4L/eticlopride, 3.15 Å).

In the crystal lattice, each receptor molecule is surrounded by four symmetry mates within the membrane-like layers. Two of the contacts are related by pure translational symmetry and mediated by cholesterol molecules. The remaining two include direct protein-protein interactions, forming parallel and anti-parallel dimers. All hydrophilic interlayer crystal contacts

occur through interactions between BRIL and extracellular loops 2 and 3 (ECL2 and 3) of A_{2A}AR. The latter interactions allowed us to fully resolve ECL2, part of which was disordered in the crystal structures of A_{2A}AR-T4L-ΔC bound to ZM241385 and UK432097.

Views along two principal lattice axes highlight low solvent content and tight packing of the receptor molecules within lipid bilayers. A_{2A}AR is shown in cyan, BRIL is green. Ordered lipids are drawn in space filling representation with carbon atoms colored in grey for lipid chains and yellow for cholesterol molecules.

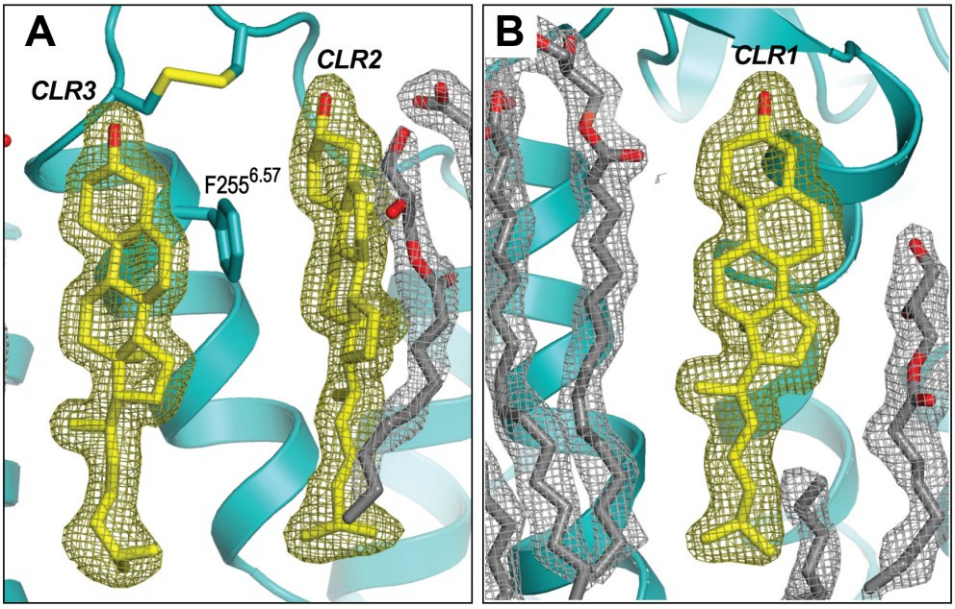

Figure S10. Electron density maps for cholesterol and lipid molecules. 2|Fo|-|Fc| electron density map contoured at 1.0 σ around cholesterols (yellow) CLR2 and CLR3 (**A**) and CLR1 (**B**). Electron density for neighboring lipids is colored grey. The receptor is depicted as a cyan ribbon. Note that Phe255$^{6.57}$ (panel **A**; represented as sticks) is sandwiched by CLR2 and CLR3.

1. R. Chu *et al.*, Redesign of a four-helix bundle protein by phage display coupled with proteolysis and structural characterization by NMR and X-ray crystallography. *Journal of molecular biology* **323**, 253 (2002).
2. J. Sambrook, E. F. Fritsch, T. Maniatis, *Molecular Cloning: A Laboratory Manual 2nd Ed.*, (Cold Spring Harbor Laboratory, Cold Spring Harbor, NY., 1989).
3. P. K. Smith *et al.*, Measurement of protein using bicinchoninic acid. *Analytical biochemistry* **150**, 76 (1985).
4. M. A. Hanson *et al.*, Profiling of membrane protein variants in a baculovirus system by coupling cell-surface detection with small-scale parallel expression. *Protein expression and purification* **56**, 85 (2007).
5. A. I. Alexandrov, M. Mileni, E. Y. Chien, M. A. Hanson, R. C. Stevens, Microscale fluorescent thermal stability assay for membrane proteins. *Structure* **16**, 351 (2008).
6. M. Caffrey, V. Cherezov, Crystallizing membrane proteins using lipidic mesophases. *Nature protocols* **4**, 706 (2009).
7. V. Cherezov, A. Peddi, L. Muthusubramaniam, Y. F. Zheng, M. Caffrey, A robotic system for crystallizing membrane and soluble proteins in lipidic mesophases. *Acta Crystallogr D Biol Crystallogr* **60**, 1795 (2004).
8. W. Minor, M. Cymborowski, Z. Otwinowski, M. Chruszcz, HKL-3000: the integration of data reduction and structure solution--from diffraction images to an initial model in minutes. *Acta Crystallogr D Biol Crystallogr* **62**, 859 (2006).
9. A. J. McCoy *et al.*, Phaser crystallographic software. *Journal of applied crystallography* **40**, 658 (2007).
10. P. Emsley, B. Lohkamp, W. G. Scott, K. Cowtan, Features and development of Coot. *Acta Crystallogr D Biol Crystallogr* **66**, 486 (2010).
11. P. Skubak, G. N. Murshudov, N. S. Pannu, Direct incorporation of experimental phase information in model refinement. *Acta Crystallogr D Biol Crystallogr* **60**, 2196 (2004).
12. M. Totrov, R. Abagyan, Flexible protein-ligand docking by global energy optimization in internal coordinates. *Proteins* **Suppl 1**, 215 (1997).
13. V. Katritch *et al.*, Analysis of full and partial agonists binding to beta2-adrenergic receptor suggests a role of transmembrane helix V in agonist-specific conformational changes. *J Mol Recognit* **22**, 307 (2009).
14. Z. G. Gao *et al.*, Differential allosteric modulation by amiloride analogues of agonist and antagonist binding at A(1) and A(3) adenosine receptors. *Biochemical pharmacology* **65**, 525 (2003).
15. Z. G. Gao, A. P. IJzerman, Allosteric modulation of A(2A) adenosine receptors by amiloride analogues and sodium ions. *Biochemical pharmacology* **60**, 669 (2000).
16. T. Halgren, Merck molecular force field I-V. *J Comp Chem* **17**, 490 (1995).
17. V. B. Chen *et al.*, MolProbity: all-atom structure validation for macromolecular crystallography. *Acta Crystallogr D Biol Crystallogr* **66**, 12 (2010).
18. F. Deflorian *et al.*, Evaluation of Molecular Modeling of Agonist Binding in Light of the Crystallographic Structure of an Agonist-Bound A(2A) Adenosine Receptor. *Journal of medicinal chemistry*, (2011).

19. P. D. Adams *et al.*, PHENIX: a comprehensive Python-based system for macromolecular structure solution. *Acta crystallographica* **66**, 213 (2010).
20. V. Cherezov, Lipidic cubic phase technologies for membrane protein structural studies. *Curr Opin Struct Biol* **21**, 559 (2011).